Co- and cross-flow extensions in an elliptical optical trap

E. Schonbrun,[1] J. Wong,[2] and K. B. Crozier[1]
[1]*School of Engineering and Applied Science, Harvard University, Cambridge, Massachusetts 02138, USA*
[2]*Schlumberger-Doll Research Center, Cambridge, Massachusetts 02139, USA*
(Received 17 November 2008; published 28 April 2009)

The extension of a particle (translational deviation) in an isotropic harmonic potential well is linearly proportional and parallel to the applied force. In an anisotropic trapping potential, the extension is instead related to the applied force by a compliance tensor. Using the focal spot of a high numerical aperture zone plate to create an elliptical potential and microfluidics to apply a calibrated force, we measure the two-dimensional extension of a trapped spherical particle. As a function of the orientation of the elliptical potential, the extension sweeps out a circular trajectory, exhibiting extensions both parallel (coflow) and perpendicular (cross flow) to the direction of the flow. The results fit well to a compliance tensor model.

DOI: 10.1103/PhysRevE.79.042401 PACS number(s): 83.80.Hj, 42.79.Ci, 47.61.−k, 87.80.Cc

The gradient force optical tweezer enables contactless manipulation of particles in suspension. In the absence of external forces, the trapped particle is centered close to the region of maximum intensity of a tightly focused laser [1,2]. Under an applied force, the particle moves to an equilibrium position, or extension, where the optical gradient force provides an equal and opposite restoring force. The force-extension relationship is approximated well by a linear spring up to distances of approximately one third of the particle diameter, at which point the restoring force is maximum [3]. By observing particle extension, femtonewton and piconewton forces [2,4] can be accurately measured provided that the optical spring constant is known. The interaction between hydrodynamic and optical forces [5–8] promises many applications of particle manipulation and sorting in microfluidic systems.

In addition to providing a linear restoring force, plane polarized optical traps have also demonstrated a torque on elliptical particles [8–12]. Rotation of the incident polarization state causes a nonspherical particle to rotate, transferring angular momentum to the trapped particle. In this case, the torque applied to the particle by the trapping laser is equal and opposite to the rotational drag applied by the fluid. The maximum torque applied to the particle occurs when the orientation of the polarization leads the orientation of the rotating particle by 45° [10]. At larger rotation rates, the trapped particle can no longer keep up, which is the rotational analog of the linear escape velocity [13].

In this Brief Report, we study a force equilibrium condition that is different from the two cited above. We trap a particle in a microfluidic channel and measure the particle extension as a function of the orientation of an elliptical potential. Using the extension as a lever arm, the optical beam is capable of applying torque to the spherical particle. The result is a two-dimensional extension that consists of components both parallel (coflow) and perpendicular (cross flow) to the applied force. The optical torque is counteracted by an opposite hydrodynamic torque, where both can be readily determined because the moment arm and the force are known. By measuring the cross-flow extension for a fixed orientation of the elliptical potential, we can measure the optical torque transferred to a particle even though the particle itself has zero net angular momentum. The two-dimensional extensions can be described by a compliance tensor that therefore also describes the linear restoring force and torque. By rotating the orientation of the elliptical potential, the particle traces out a circular trajectory because the components of the extension vary sinusoidally in quadrature.

We perform optical trapping of 1.1 μm latex beads using a 976 nm diode laser focused by a 1.30 numerical aperture (NA) gold-on-glass zone plate [14], shown in Figs. 1(a) and 1(b). The experimental setup to load, trap, and measure bead positions is further described in Ref. [14]. The zone plate is fabricated on the inner chamber wall of a polydimethylsiloxane (PDMS) based microfluidic channel. Beads are trapped in the focal volume, 2.9 μm $(4\lambda/n_{\text{water}})$, above the glass substrate that seals the channel. Using a syringe pump to generate pressure driven flow in the channel, we apply calibrated forces and measure the trapped particle extension.

Large numerical aperture focusing elements produce spots with elliptical intensity distributions [15]. The ellipticity is caused by an axial electric field component that elongates the beam in the direction parallel to the incident linear polarization. Fresnel zone plates have an apodization factor that enhances the axial field component, producing a more elliptical

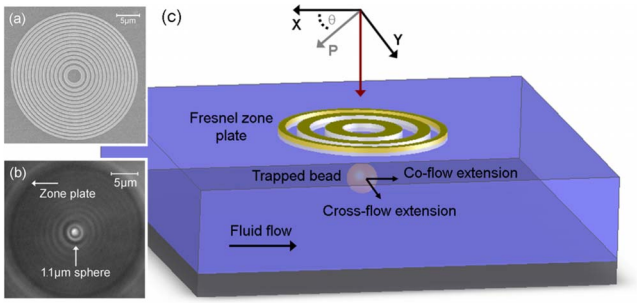

FIG. 1. (Color online) Fresnel zone plate tweezer integrated with microfluidics. (a) Scanning electron micrograph of the gold-on-glass zone plate. (b) Microscope image of a 1.1 μm sphere trapped by the zone plate tweezer. (c) Schematic of the experimental setup. The zone plate is illuminated by a laser beam propagating in **Z** that slightly overfills the zone plate aperture. The orientation of the elliptical potential is controlled by rotating the incident polarization **P**, where **X** is parallel to the fluid flow (coflow) and **Y** is perpendicular to the fluid flow (cross flow). **P** is in the **X**-**Y** plane.

focal spot than an aplanatic lens [16]. Previously, we have shown that the elliptical focal spot produced by a high NA zone plate produces an elliptical trapping potential [17] that has higher anisotropy than that produced by an aplanatic objective lens [18]. Using a half-wave plate, the orientation of the elliptical trapping potential can be continuously rotated. Figure 1(c) shows a diagram of the experiment. A fluid drag force is applied in the plane of the elliptical trapping potential. Therefore, by rotating the incident polarization, the major and minor axes of the elliptical potential can be oriented with respect to the applied force.

In order to calibrate the applied fluid drag force, we first measure the flow velocity at the location of the trapped bead. This is done by observing the motion of particles in the flow field at a variety of flow rates [6,7]. We perform position measurements by evaluating the image centroid of fluorescence images using video microscopy. Particles are placed at the position of interest by trapping them with the zone plate and then released by blocking the trapping laser. By measuring the time, Δt, it takes for each particle to travel across the field of view (30 μm), we can determine the local velocity. The uncertainty in velocity determination using this method is proportional to $1/\sqrt{\Delta t}$. We find that the flow velocity scales linearly with flow rate, but there is additional uncertainty in the velocity fields we believe due to pressure transients in the channel and inlet and outlet tubings. For a laser power of 50 mW, the zone plate tweezer can trap particles in flows of velocities up to 225 μm/s, the linear escape velocity of the tweezer. Using these calibrated drag forces, we can now investigate the particle extension under an applied force as a function of the orientation of the elliptical potential.

The extension is related to applied force by the inverse of the stiffness, which we term the "optical compliance." We restrict our investigation to the two-dimensional plane transverse to the trapping laser propagation direction. The force-extension relation follows Hooke's law,

$$\vec{F} = \overleftrightarrow{K} \cdot \vec{r}, \tag{1a}$$

$$\vec{r} = \overleftrightarrow{K}^{-1} \cdot \vec{F} = \overleftrightarrow{L} \cdot \vec{F}, \tag{1b}$$

where $\vec{F}$ is the applied Stokes drag force vector, equal to $6\pi\eta a\vec{v}$, $\overleftrightarrow{K}$ is the optical stiffness tensor, $\overleftrightarrow{L}$ is the optical compliance tensor, $\vec{r}$ is the extension vector, η is the viscosity, a is the sphere radius, and $\vec{v}$ is the fluid velocity. Figure 2 shows the measured coflow extension when the elliptical potential has its major axis parallel to the applied force in blue (dark) and perpendicular to the applied force in red (light). The extension divided by the applied force gives the magnitude of the appropriate element of the optical compliance tensor $\overleftrightarrow{L}$. These two cases represent the two diagonal terms of the compliance matrix when the force is applied along one of the two principal axes of the elliptical potential. In this case, the optical trap applies a restoring force that is parallel to the direction of the applied force from the flow. There is no cross-flow extension, and consequently no applied optical torque. In the measurement coordinate frame, the extension is related to the optical compliance by

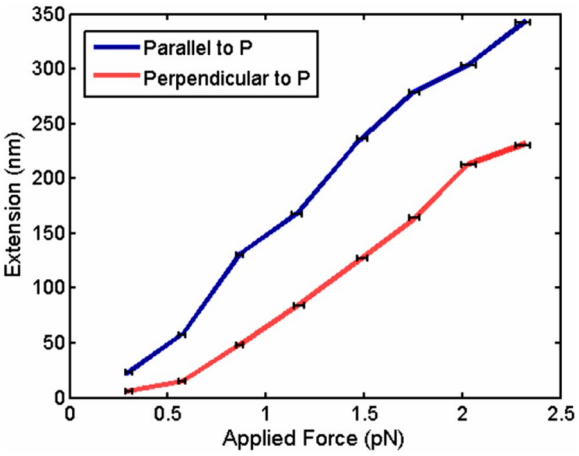

FIG. 2. (Color online) Force coflow extension curves. Extension is measured along the flow direction when the polarization of the laser beam incident on the zone plate tweezer is parallel to the flow in blue (dark) and perpendicular to the flow in red (light). Uncertainty in the applied force arises from uncertainty in the velocity field applied by the syringe pump. Uncertainty in the extension is below 3 nm and is not plotted. The optical compliance at 1.2 pN for parallel polarization is approximately twice the optical compliance for perpendicular polarization.

$$\begin{bmatrix} r_x \\ r_y \end{bmatrix} = \begin{bmatrix} \cos\theta & -\sin\theta \\ \sin\theta & \cos\theta \end{bmatrix} \begin{bmatrix} L_{\text{par}} & 0 \\ 0 & L_{\text{perp}} \end{bmatrix} \begin{bmatrix} \cos\theta & \sin\theta \\ -\sin\theta & \cos\theta \end{bmatrix} \times \begin{bmatrix} F_x \\ 0 \end{bmatrix}, \tag{2}$$

where L_{par} is the optical compliance for forces and extensions parallel to the incident polarization, L_{perp} is the optical compliance for forces and extensions perpendicular to the incident polarization, F_x is the fluid drag force, r_x is the coflow extension, and r_y is the cross-flow extension. The rotation matrices rotate the force into the principal coordinate frame of the elliptical trapping potential and then back into the observation coordinate frame. The blue (dark) curve in Fig. 2 plots r_x for a θ=0° rotation and the red (light) curve is r_x for a θ=90° rotation, where r_y in both cases is small. The compliance is not completely constant over the range of applied forces. Instead, the trap is stiffer and more elliptical at small extensions. In order to investigate the off-diagonal compliance terms, we operate at a fluid force of 1.2 pN, corresponding to a flow velocity of 115 μm/s. At this point in the force-extension curve, L_{perp} is 72 nm/pN and L_{par} is 145 nm/pN.

For an arbitrary rotation angle, $\overleftrightarrow{L}$ contains on- and off-diagonal terms that couple the force in the flow direction to co- (L_{xx}) and cross-flow (L_{xy}) extensions. Figure 3 shows extension data as a function of time during the application of a 1.2 pN fluid drag force, where each panel corresponds to a different orientation of the elliptical potential. Extension data are taken at 30 Hz for a total of 10 s. The syringe pump is turned on at approximately 4 s and the channel and inlet/outlet tubing take approximately 2 s to come to equilibrium in pressure. The insets of Fig. 3 schematically illustrate the

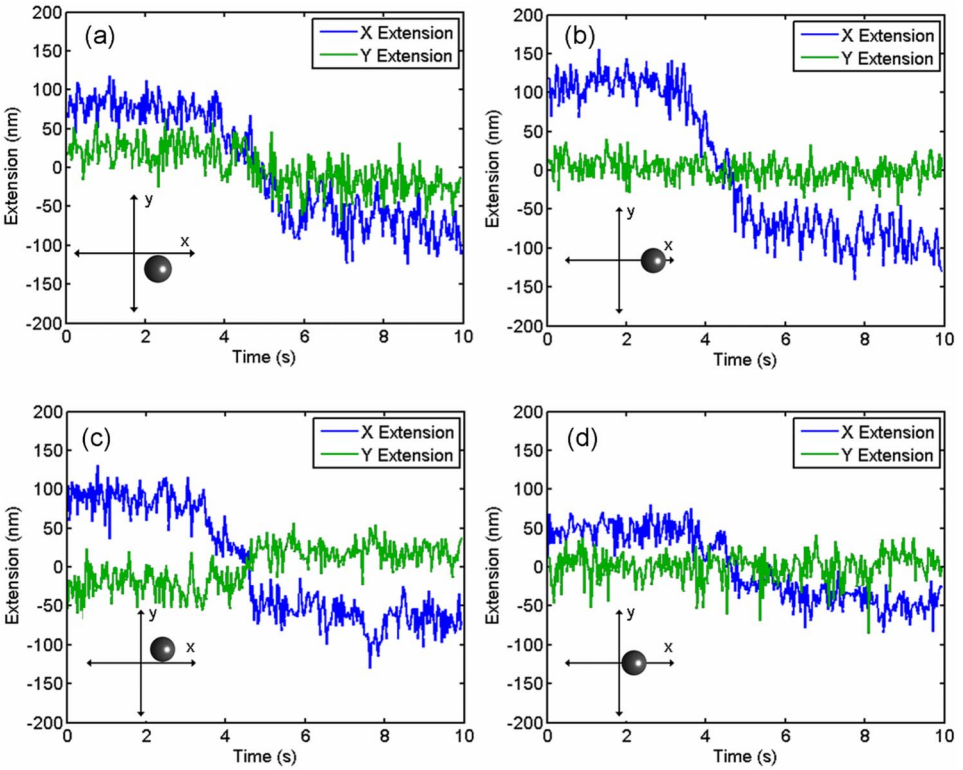

FIG. 3. (Color online) Extension time traces. Coflow extension in blue (dark) and cross-flow extension in green (light) for four different orientations of the elliptical potential, −45°, 0°, 45°, and 90° for (a), (b), (c), and (d), respectively. The orientation angle describes the relative angle between the fluid flow and the polarization angle or the major axis of the elliptical potential. At 4 s, the syringe pump is turned on and after reaching equilibrium applies a force of 1.2 pN to the trapped bead. Insets illustrate particle position after equilibrium is reached. For orientations of 45° and −45°, a cross-flow extension is resolvable that is pointed in opposite directions. An offset has been added to each extension trace so that each has a mean value of zero.

particle positions after equilibrium has been reached. For a sampling rate of 30 Hz, particle positions are uncorrelated and using averaging we can obtain measurement accuracy of 3.1 and 4.3 nm/$\sqrt{\text{Hz}}$ for the directions perpendicular and parallel to the incident polarization, respectively. The extension is found by averaging the position of the first 100 samples and then subtracting by the average position of the last 100 samples. The 0° and 90° cases correspond to the cases in Fig. 2 where the force is applied along the principal axes of the potential and there is no cross-flow extension. For the 45° and −45° potential orientations, the cross-flow extension is clearly resolvable and points in both the positive (45° orientation) and negative (−45° orientation) **Y** directions.

The cross-flow extension can be accurately predicted by the off-diagonal terms of L. By multiplying through Eq. (2), the off-diagonal term (L_{xy}) can be shown to be $L_{\text{par}} \cos\theta \sin\theta - L_{\text{perp}} \cos\theta \sin\theta$. The maximum value for the cross-flow extension occurs at a 45° orientation, and in our case where $L_{\text{par}} \approx 2L_{\text{perp}}$, the off-diagonal compliance is $0.5L_{\text{perp}}$. We observe 47 and -42 ± 3 nm cross-flow extensions for the 45° and −45° potential orientations, respectively. The measured coflow extension for the perpendicular polarization orientation is 95 nm and therefore agrees well with the compliance tensor model. Plane polarization induced torque has also been shown to peak when the relative angle between the incident polarization and an elongated trapped particle is 45° [10,11], which in mechanics is called the direction of maximum shear.

Figure 4 plots the equilibrium position under a constant 1.2 pN force for 12 orientations of the elliptical potential, obtaining by rotating the polarization of the beam incident on the zone plate. The data in blue (dark) are taken at 15° increments of the polarization, with the same 1.1 μm sphere used in all experiments. By evaluating Eq. (2) and using $\Delta L = L_{\text{par}} - L_{\text{perp}}$ and $L_{\text{av}} = (L_{\text{par}} + L_{\text{perp}})/2$, the coflow compliance can be written as $L_{xx} = L_{\text{av}} + \Delta L \cos(2\theta)/2$ and the cross-flow compliance as $L_{xy} = \Delta L \sin(2\theta)/2$. Due to the fact that

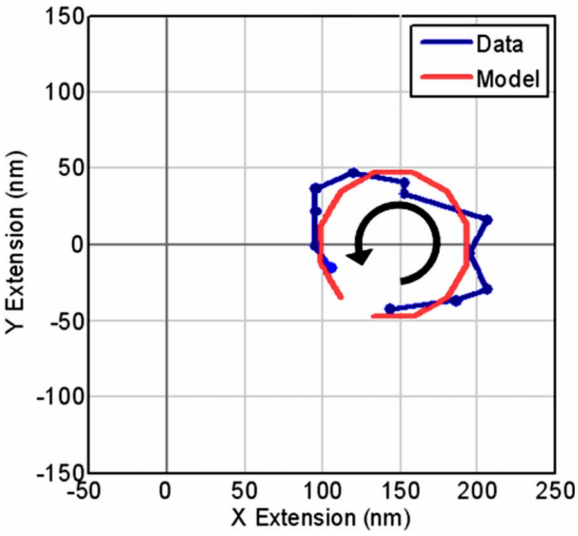

FIG. 4. (Color online) Equiforce equilibrium positions. For a constant 1.2 pN applied force, the equilibrium position as a function of the orientation of the elliptical potential is plotted. Each data point in blue (dark) corresponds to a 15° counterclockwise rotation of the trapping potential, starting at an orientation of θ=45°. The data are fit to the optical compliance tensor model which predicts a circular trajectory in red (light). The origin of the two-dimensional extension is the position of the sphere without an applied fluid force. Uncertainty in the extension measurements is below 3 nm, which is the size of the plotted dots.

they are in quadrature, the extension traces out a circular trajectory with a radius of $\Delta L/2$. The extension curve completes one revolution on rotating the potential by 180° or rotating the half-wave plate by 90°. The measured trajectory is slightly elliptical, likely to result from the fact that the dichroic beam splitter for the trapping laser induces some ellipticity in the incident polarization state. Using an applied linear force, we have shown that we can revolve a spherical particle by rotating the incident linear polarization in the back aperture of the focusing lens. The magnitude of this effect is proportional to the ellipticity of the compliance ΔL, consequently going to zero for an isotropic potential.

The center of our coordinate system is taken to be the location where the sphere is trapped in the absence of flow. For a given cross-flow extension and under a constant fluid linear drag force, the fluid induced torque is $\tau = r \times F$. In order for the sphere to be in equilibrium, the optical torque must be canceled by an equal and opposite hydrodynamic torque. Consequently, measuring the cross-flow extension is a simple method to evaluate the applied optical torque. The torque applied in our experiment at a 45° potential orientation is 56 pN nm. This value is comparable to other experiments demonstrating torque using plane polarization rotation [10,11] and larger than torque generated by orbital angular momentum [8]. By controlling the relative orientation between the major axis of the potential and the applied fluid force, we can apply and measure torques of this systems as small as 3 pN nm/$\sqrt{\text{Hz}}$.

Although they are both electromagnetic forces, linear restoring force and torque are often considered separately and are studied in different experiments. By displacing the equilibrium position of a trapped particle using fluid flow, we have shown that both linear force and torque can be measured on a spherical particle in the same experiment. The coflow extension is a balance of the linear restoring force and Stokes drag force and the cross-flow extension is a balance of optical and hydrodynamic torque. Both are described by an optical compliance tensor. The contributions of the linear force and torque can be controlled by rotating the incident linear polarization relative to the applied fluid force. By continuously rotating the incident polarization, we have demonstrated a method to revolve a particle along an orbit with a diameter of ~100 nm. The diameter of the revolution can be increased either by applying a larger fluid force or by using a more elliptical focal spot.

ACKNOWLEDGMENTS

This work was supported by Schlumberger-Doll Research, the Defense Advanced Research Projects Agency (DARPA) and the National Science Foundation (NSF). Fabrication work was carried out at the Harvard Center for Nanoscale Systems, which is supported by the NSF.

[1] A. Ashkin, J. M. Dziezic, J. E. Bjorkholm, and S. Chu, Opt. Lett. **11**, 288 (1986).
[2] K. C. Neuman and S. M. Block, Rev. Sci. Instrum. **75**, 2787 (2004).
[3] R. M. Simmons, J. T. Finer, S. Chu, and J. A. Spudich, Biophys. J. **70**, 1813 (1996).
[4] A. Ashkin, Proc. Natl. Acad. Sci. U.S.A. **94**, 4853 (1997).
[5] T. T. Perkins, D. E. Smith, R. G. Larson, and S. Chu, Science **268**, 83 (1995).
[6] G. J. L. Wuite, R. J. Davenport, A. Rappaport, and C. Bustamante, Biophys. J. **79**, 1155 (2000).
[7] R. DiLeonardo, J. Leach, H. Mushfique, J. M. Cooper, G. Ruocco, and M. J. Padgett, Phys. Rev. Lett. **96**, 134502 (2006).
[8] G. Volpe and D. Petrov, Phys. Rev. Lett. **97**, 210603 (2006).
[9] M. E. J. Friese, T. A. Nieminen, N. R. Heckenberg, and H. Rubinsztein-Dunlop, Nature (London) **394**, 348 (1998).
[10] A. I. Bishop, T. A. Nieminen, N. R. Heckenberg, and H. Rubinsztein-Dunlop, Phys. Rev. A **68**, 033802 (2003).
[11] P. Galajda and P. Ormos, Opt. Express **11**, 446 (2003).
[12] C. Lin, I. Wang, B. Dollet, and P. L. Baldeck, Opt. Lett. **31**, 329 (2006).
[13] A. Ashkin, Biophys. J. **61**, 569 (1992).
[14] E. Schonbrun, C. Rinzler, and K. B. Crozier, Appl. Phys. Lett. **92**, 071112 (2008).
[15] B. Richards and E. Wolf, Proc. R. Soc. London, Ser. A **253**, 358 (1959).
[16] N. Davidson and N. Bokor, Opt. Lett. **29**, 1318 (2004).
[17] E. Schonbrun and K. B. Crozier, Opt. Lett. **33**, 2017 (2008).
[18] A. Rohrbach, Phys. Rev. Lett. **95**, 168102 (2005).